Impact of Human Activities on the Concentrations of Biogenic Elements in the Natural Environment of the Yangtze River Basin

Ruichen Zheng

Nanjing Foreign Language School, Nanjing, China

Keywords: Biogenic elements, Human activities, Total suspended particulate (tsp), Water, Soil, Yangtze river basin

Abstract: Biogenic elements play an essential role in maintaining human livelihoods, but too many biogenic elements can also harm the environment. Human activities can change the concentrations of biogenic elements in the natural environment, especially in river basin areas that breed countless human civilizations. Although the Yangtze River is the largest river in Asia, few studies have focused on biogenic elements in the atmosphere, water, and soil of the entire Yangtze River Basin (YRB) simultaneously. This study selects nine locations in the YRB with different levels of economic development, as indicated by the level of GDP density and population density. Samples of atmospheric total suspended particulate (TSP), water, and soil were collected. The physical and chemical properties of biogenic elements present in these samples (carbon, nitrogen, sulfur, and phosphorus) were further analyzed. The resulting concentrations changes vary significantly among TSP, water, and soil with changes in human activities intensity. With the increasing human activities intensity, the concentration in TSP increased first to a peak before falling, conforming to the inverted U curve of environmental pollution, indicating that the peak period of air pollution in the YRB has passed. The mathematical model established in this study shows that the per capita GDP of 37,092 Yuan is the turning point for air quality to change from deterioration to improvement, which conforms with China's per capita GDP and air quality in recent years. The level of water pollution in the YRB is currently at its peak stage. The concentration in the soil is still increasing but is currently too low to cause environmental hazards. With economic developments, people will improve environmental quality in the sequence of air, water, and soil. This study has important implications for understanding the relationship between human activities and environmental quality to alert the government of environmental pollution prevention and control work.

1. Introduction

Biogenic elements refer to the major elements required by living organisms (Song, 2010), including carbon (C), nitrogen (N), sulfur (S), phosphorus (P), oxygen (O), and hydrogen (H). Proteins, the crucial components of all human cells and tissues, are mainly composed of these essential elements. The concentration of biogenic elements in the natural environment can significantly affect biodiversity and ecosystem succession (Gorham et al., 1979). In this way, people can increase crop yields by applying nutrients such as N and P (Lu and Tian, 2017). However, unregulated biogenic elements can also bring adverse effects: vast amounts of greenhouse gas emissions can cause global warming (Daniel and Ahuja, 1990); N and S oxides and their corresponding nitrates and sulfates are common atmospheric pollutants (Streets and Waldhoff, 2000; Huang et al., 2014); excessive plant nutrients such as N and P can lead to water eutrophication (Smith and Schindler, 2009). Under such circumstances, studying the concentration of biogenic elements such as C, N, S, and P in the natural environment and their responses to human activities are essential prerequisites for utilizing the functionality and avoiding the harm of biogenic elements.

Rivers are critical hydrological cycle pathways and channels for sediments, salts, and chemical elements to enter lakes and oceans (Humborg et al., 2007). Rivers are of great significance to human beings (Karr and Chu, 2000): in addition to providing water for living and agriculture, they also serve for navigation, flood control, aquaculture, tourism, and climate regulation. Historically, human beings and their social and ecological systems have been interdependent and inseparable

  DOI: 10.25236/edssr.2022.033

from rivers (Holme, 2010). For example, the four ancient civilizations all originated in river areas. In recent centuries, along with the dramatic population increment, accelerated urbanization, and increased intensity of industrial and agricultural production activities, large amounts of anthropogenic substances have been discharged into environmental media such as the atmosphere, water bodies, and soil. This unprecedented situation has brought about critical impacts on the natural environment of water basins, including atmospheric pollution (Violante et al., 2006), water eutrophication (Pinto et al., 2012), and soil contamination (Galitskova and Murzayeva, 2016). In addition, nutrients and pollutants can migrate and transform among various environmental media, making it critical to consider different environmental media when solving the problems above.

The largest river in Asia, the Yangtze River, runs through Nanjing, the author's hometown. It has played a crucial role in Nanjing's urban civilization's origin and development. The Yangtze River originates in the Tanggula Mountains on the Tibetan Plateau and flows through 11 provinces, autonomous regions, and municipalities before flowing into the East China Sea (Zhuo et al., 2020). Spanning three major economic zones in western, central, and eastern China, the YRB includes 19 provinces, autonomous regions, and municipalities, covers 1.8 million square kilometers, accounts for 18.8% of China's land area, and contains a population of nearly 400 million (Zhang et al., 2020). The Yangtze River has great zoning for human activities, with both ecologically sound remote areas and densely populated megacities: the upper reaches are sparsely populated, but the middle and lower reaches are significantly anthropogenic. Thus, the large and clearly zoned YRB provides an ideal place for comparatively studying human activities' impact on the natural environment. However, few studies simultaneously focus on the biogenic elements in the air, water, and soil in the YRB.

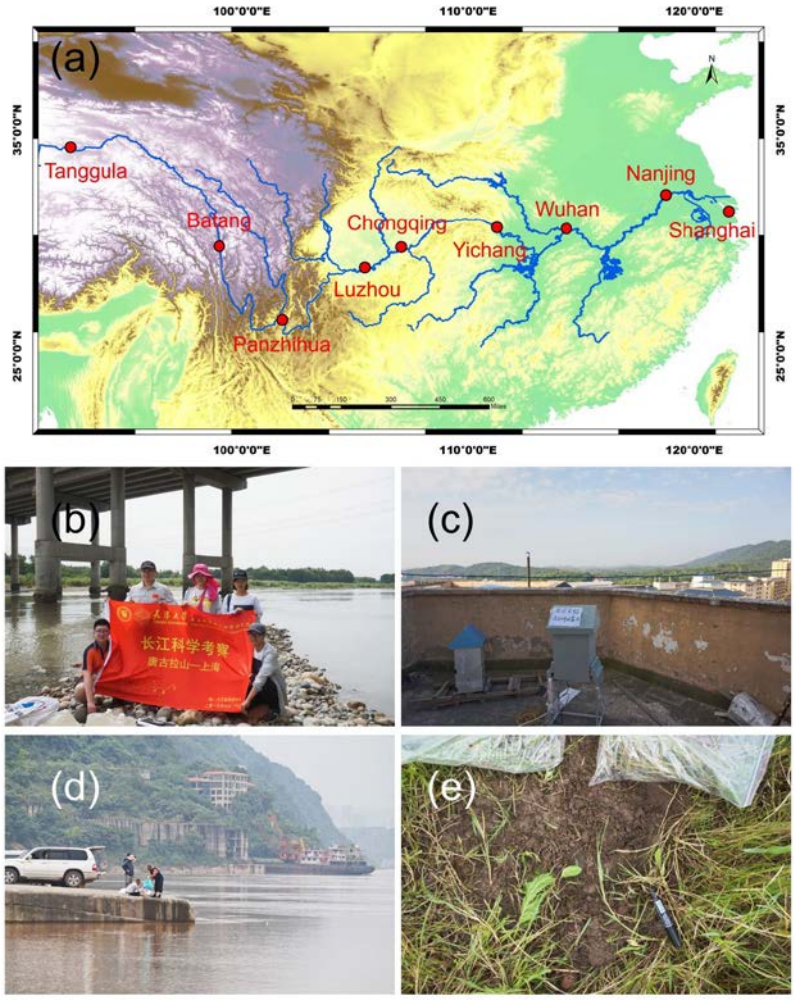

Figure 1. (a) A map of YRB showing the nine sampling sites we selected; (b) A group photo of the 2019 Yangtze River scientific expedition team; (c–e) Pictures showing (c) TSP samples collected using a high-volume air sampler, (d) water and (e) soil samples collection.

This study plans to collect atmospheric particulate matter, water, and soil samples

from areas with different land-use patterns, population size and density, total economic volume, and industrial and agricultural output in the YRB. The samples were further tested in the laboratory for ammonium (NH_4^+), nitrate (NO_3^-), sulfate (SO_4^{2-}), phosphate (PO_4^{3-}), and other anions and cations, water-soluble organic carbon (WSOC), total dissolved nitrogen (TDN), spectral characteristics, total carbon (TC) and their isotopic compositions ($\delta^{13}C$), total nitrogen (TN) and their isotopic compositions ($\delta^{15}N$) to analyze the effects of human activities on the concentration of biogenic elements in the natural environment. The relationship between the degree of economic development and the quality of the ecological environment is explored.

2. Methods

2.1 Sites Description and Sample Collection

The Yangtze River originates from the Mountain Tanggula on the Qinghai-Tibet Plateau. The mainstream flows through 11 provinces, autonomous regions, or municipalities, including Qinghai, Tibet, Sichuan, Yunnan, Chongqing, Hubei, Hunan, Jiangxi, Anhui, Jiangsu, and Shanghai (Zhuo et al., 2020), and eventually into the East China Sea to the east of Chongming Island (Fig. 1a). A research team from Tianjin University conducted a scientific investigation on the mainstream and main tributaries of the Yangtze River in the summer of 2019 (from June to August), and I got involved in a part of the fieldwork (Fig. 1b). In this study, total suspended particulate (TSP), water, and soil samples from nine regions were chosen for analyses: Tanggula Town in Qinghai Province, Batang County, Panzhihua City and Luzhou City in Sichuan Province, Chongqing Municipality, Wuhan City in Hubei Province, Nanjing City in Jiangsu Province, and Shanghai Municipality. Basic information of the nine locations is listed in Table 1.

TSP samples were collected onto preheated (450 °C, 6h) quartz fiber filters (2500QAT‐UP, Pallflex) using a high-volume air sampler (Tisch 4010126, USA, Fig. 1c) at an airflow rate of ~1.1 m^3 min^{-1} and for ~12 h for each sample (Wu et al., 2021). Water samples were collected in the water bag (Fig. 1d), after which impurities were filtered out with a peristaltic pump and placed in a brown bottle. Soil samples (Fig. 1e) were collected using a stainless steel shovel and placed in sealed plastic bags around the water sampling sites. After collection, all samples were placed in a refrigerator at –20 °C and mailed to the laboratory for further analyses.

Table 1. Area, population size and density, gross domestic product (GDP, Yuan), and GDP density of the nine selected cities along the Yangtze River in 2019 (Qinghai Provincial Bureau of Statistics & Survey Office of the National Bureau of Statistics in Qinghai, 2020; Sichuan Provincial Bureau of Statistics & Survey Office of the National Bureau of Statistics in Sichuan, 2020; Chongqing Municipal Bureau of Statistics & Survey Office of the National Bureau of Statistics in Chongqing, 2020; Hubei Provincial Bureau of Statistics & Survey Office of the National Bureau of Statistics in Hubei, 2020; Jiangsu Provincial Bureau of Statistics & Survey Office of the National Bureau of Statistics in Jiangsu, 2020; Shanghai Municipal Bureau of Statistics & Survey Office of the National Bureau of Statistics in Shanghai, 2020).

No.	Location	Area (10^4 km^2)	Population (10^4)	Population density (km^{-2})	GDP (100 million)	GDP density (100 million km^{-2})
1	Tanggula	4.78	0.19	0.04	4.21	0.000088
2	Batang	0.82	5.16	6.29	16.06	0.001959
3	Panzhihua	0.74	121	164.05	1010	0.137
4	Luzhou	1.22	509	416.83	2081	0.171
5	Chongqing	8.24	3404	413.06	25003	0.303
6	Yichang	2.10	414	197.04	4461	0.212
7	Wuhan	0.86	1121	1303.72	16223	1.886
8	Nanjing	0.66	850	1287.88	14030	2.126
9	Shanghai	0.63	2428	3854.19	38155	6.056

2.2 Chemical and Isotopic Analyses

2.2.1 Pre-Treatment

A filter aliquot of each TSP sample was cut with a specific size using a filter cutter and placed in a 50 mL extraction flask, after which 10 mL ultrapure water was added. The extraction was placed in an ultrasonic extractor for 10 minutes and filtered with a 0.45 μm filter membrane before placing in another extraction flask (Fig. 2a, Wu et al., 2021). The operation was repeated three times. The water samples were filtered with Whatman glass fiber membranes (Karanfil et al., 2003), which were burned beforehand in a muffle furnace at 450 °C for 6 hours to remove organic matter that might be adsorbed on the membranes. Three grams of each air-dried soil sample was weighed and placed in a 50 mL centrifuge tube, and 30 mL of ultrapure water was added according to the ratio of water to soil = 10: 1. The samples were then placed in a constant temperature shaker set at 25 °C, oscillated at 200 r min^{-1} for 16 h, and further centrifuged at a speed of 4000 r min^{-1} for 20 minutes before the supernatant was filtered through a 0.45 μm filter membrane (Haygarth et al., 1997).

2.2.2 Wsoc and Tdn Analyses

WSOC and TDN were analyzed using Total Organic Carbon Analyzer (TOC Analyzer, Shimadzu, Japan, Fig. 2b, Volk et al., 2012). Before sample analyses, the instruments were calibrated with potassium hydrogen phthalate and potassium nitrate, respectively.

2.2.3 Anion and Cation Contents

The water and TSP filter extracts can be tested directly on the machine after filtration. The soil extracts passed through a processed SPE cartridge (5 mL chromatographic grade methanol + 15 mL ultrapure water for cleaning). The first 5 mL samples were discarded before obtaining samples for analysis. Water-soluble ions, including NH_4^+, NO_3^-, SO_4^{2-} and PO_4^{3-} were detected by Ion Chromatography (IC, Thermo Fisher, Fig. 2c, Dawood and Sanad, 2014), and the standard solution of each ion was used for calibration before measurement.

2.2.4 Excitation-Emission-Matrix Spectra

The Excitation-Emission-Matrix (EEM) Spectra of the treated aqueous solution was analyzed with a fluorometer (Fluoromax-4, Horiba, Fig. 2d). The emission wavelength, excitation wavelength, and fluorescence intensity were obtained (Chai et al., 2018; Cheng et al., 2020).

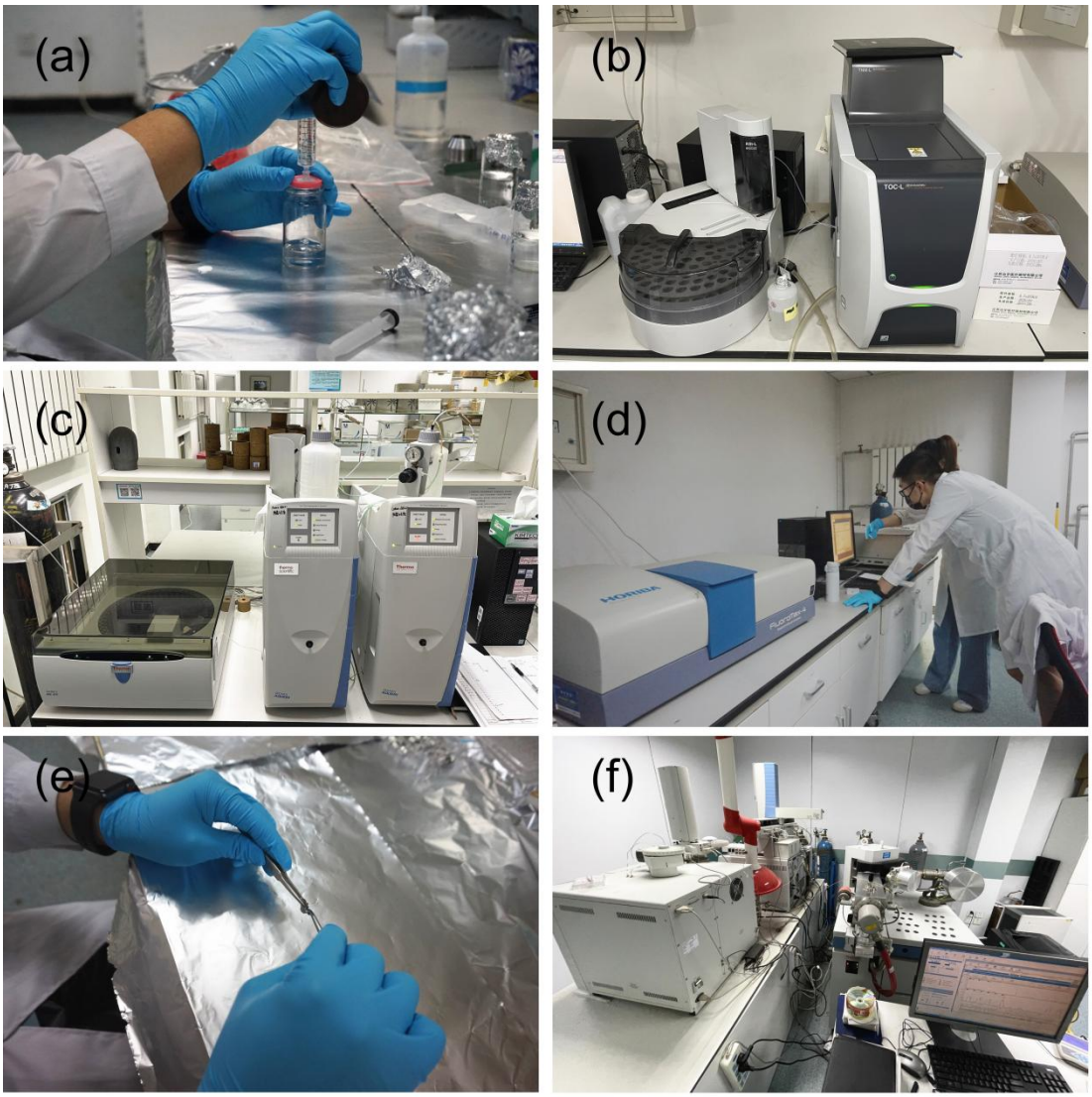

Figure 2. Pre-treatment and chemical and isotopic analyses. (a) Filtration of solution; (b) Total Organic Carbon Analyzer (TOC Analyzer); (c) Ion Chromatography (IC); (d) Excitation-Emission-Matrix (EEM) Spectrophotometer; (e) Wrapping samples in small tin cups; (f) Elemental Analyzer coupled with Stable Isotope Mass Spectrometer.

2.2.5 Concentrations and Stable Isotopic Compositions of Tc and Tn

A filter aliquot of each TSP (Fig. 2e) was combusted at 1000 °C using a FLASH 2000 HT Elemental Analyzer (Thermo Fisher) for TC and TN analyses. For stable C and N isotope analyses, the gases were sent to Isotope-Ratio Mass Spectrometry (IRMS) MAT 253 (Thermo Fisher, Fig. 2f, Wu et al., 2021). Stable isotope ratios were expressed in δ notation as the deviation from standards in parts per thousand (‰):

$$\delta^{13}\mathrm{C} = [(R_{sample} / R_{standard})] \times 1000 \quad (1)$$

where R refers to the ratio $^{13}C / {}^{12}C$, the $R_{standard}$ value is based on Vienna Pee Dee Belemnite (V-PDB), and

$$\delta^{15}\mathrm{N} = [(R_{sample} / R_{standard})] \times 1000 \quad (2)$$

where R represents the ratio $^{15}N / {}^{14}N$, the $R_{standard}$ value is based on atmospheric air nitrogen (N_2-atm).

3. Results and Discussion

Fig. 3 shows the population and GDP data of the nine selected locations. We can notice that these

places vary significantly, representing different levels of anthropogenic influences of the YRB. Tanggula in Qinghai Province and Batang in Sichuan Province are located on the Qinghai-Tibet Plateau, both of which belong to the source regions of the Yangtze River – locally called Tuotuo River and Jinsha River, respectively. These two regions are sparsely populated and have a more pristine natural environment. Panzhihua, Luzhou, and Yichang are cities with medium population and economic scale. Although Chongqing has a large population and a high GDP, it has a large area, making its population density and GDP density comparable to those of Panzhihua, Luzhou, and Yichang. Located in the middle and lower reaches of the Yangtze River, Wuhan and Nanjing are the capital cities of Hubei Province and Jiangsu Province, with developed economies and a population of about 10 million. Shanghai, located at the mouth of the Yangtze River with over 20 million people, has a highly developed economy that makes it a world-renowned megacity. Based on the population density and GDP density, we conclude that the degree of human activities influence is: Shanghai > Wuhan and Nanjing > Panzhihua, Luzhou, Chongqing, and Yichang > Tanggula and Batang.

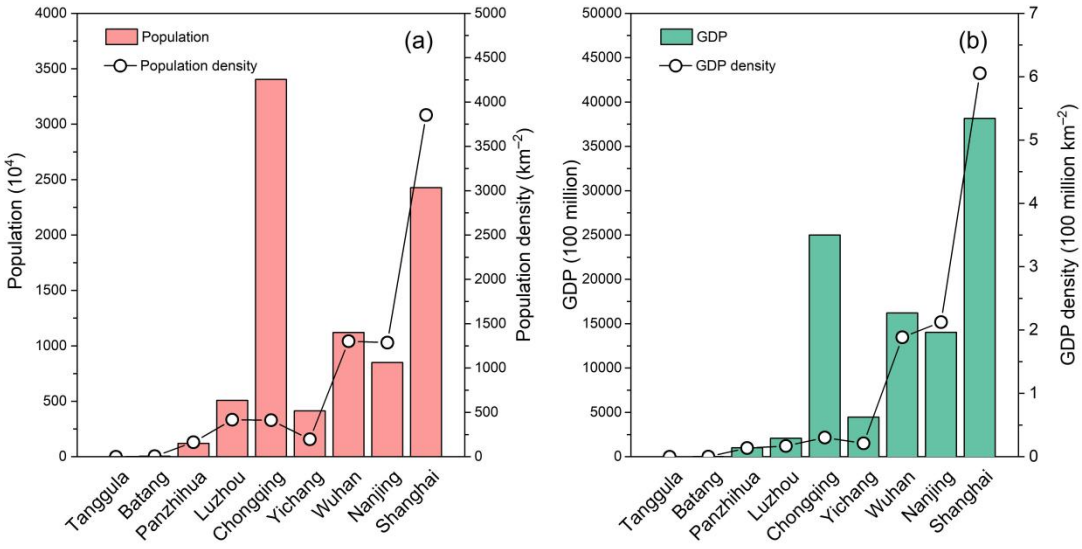

Fig.3 (a) Population Size and Density, (B) Gross Domestic Product (Gdp, Yuan) and Gdp Density of the Nine Selected Cities Along the Yangtze River in 2019.

3.1 Tsp

Fig. 4 indicates the relationships between the leading test indicators of TSP and the GDP density and population density. An excellent quadratic function relationship is presented for TC, WSOC, TN, and TDN in TSP. With the increase of GDP and population density, these indicators first show an upward trend and soon decrease after reaching a peak. In addition to the diffusion condition discrepancies of atmospheric pollutants due to natural causes such as terrain, climate, and proximity to the ocean, human activities play a critical role in atmospheric C and N, the primary contents of TSP. Its increment in the first stage is bought by the increasing amounts of pollutants emitted owing to economic development. However, when the economy develops to a certain level, society's desire for air quality will increase dramatically, soon outweighing the industrial benefit. Under such circumstances, the government will invest more funds to improve air quality, pushing towards a decrease in C and N content. This is in accordance with the Kuznets inverted U-shaped curve hypothesis and the inverted U curve of environmental pollution: in the process of industrialization, along with the increase of GDP per capita, the degree of environmental pollution will first increase then decrease (Cole et al., 1997; Dasgupta et al., 2002). If G, P, and S mean GDP, population size, and the area of the cities (towns), respectively, Eqs. 3–10 are the proper functions.

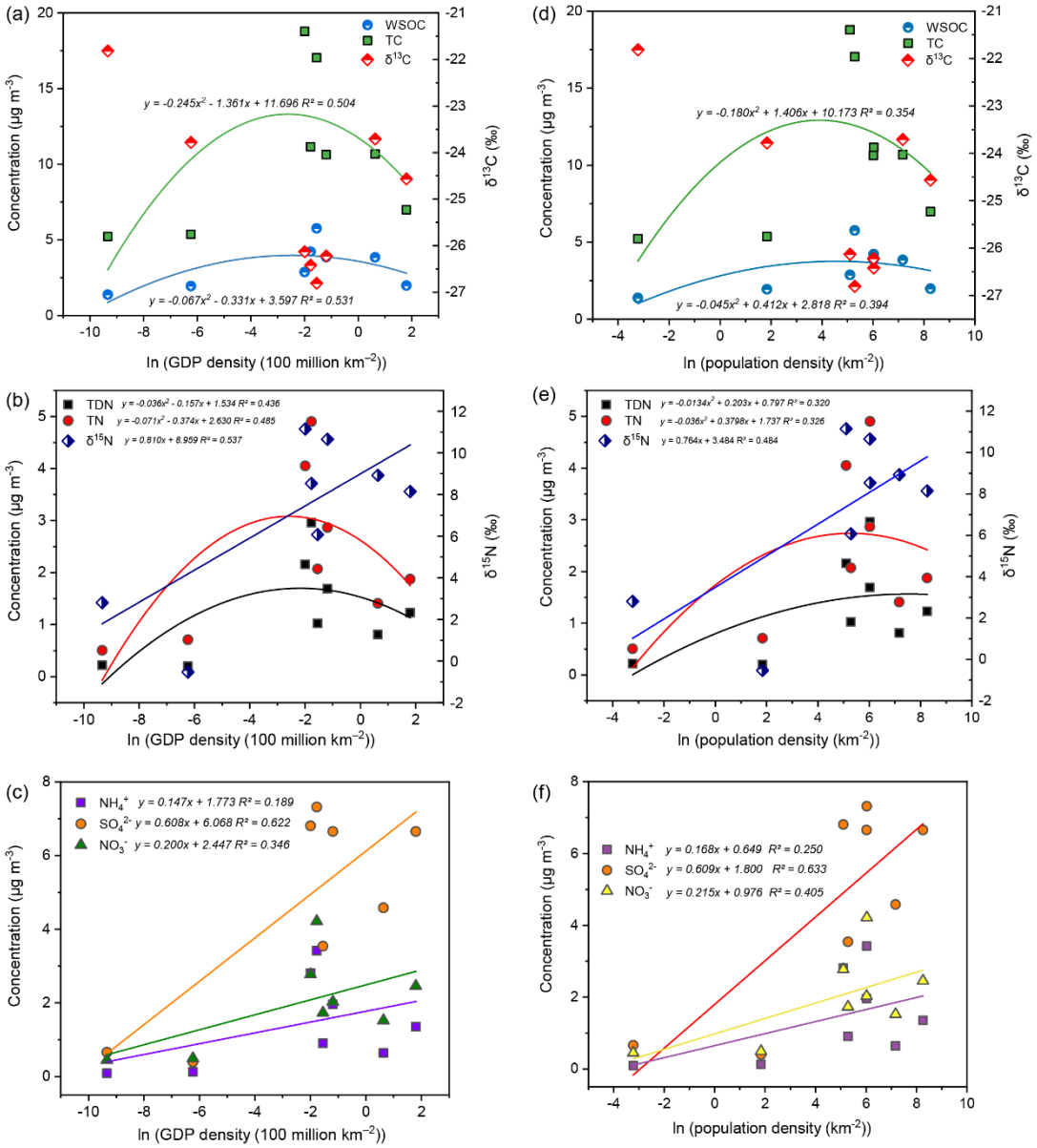

Figure 4 Relationships between (a) WSOC, TC, δ13C-TC, (b) TDN, TN, δ15N, (c) NH4+, SO42–, NO3– in TSP and ln (GDP density); (d) WSOC, TC, δ13C-TC, (e) TDN, TN, δ15N, (f) NH4+, SO42–, NO3– in TSP and ln (population density).

$$[TC] = -0.245\left[\ln\left(\frac{G}{S}\right)\right]^2 - 1.361ln\left(\frac{G}{S}\right) + 11.696 \quad (3)$$

$$[TC] = -0.180\left[\ln\left(\frac{P}{S}\right)\right]^2 + 1.406ln\left(\frac{P}{S}\right) + 10.173 \quad (4)$$

$$[WSOC] = -0.067\left[\ln\left(\frac{G}{S}\right)\right]^2 - 0.331ln\left(\frac{G}{S}\right) + 3.597 \quad (5)$$

$$[WSOC] = -0.045\left[\ln\left(\frac{P}{S}\right)\right]^2 + 0.412ln\left(\frac{P}{S}\right) + 2.818 \quad (6)$$

$$[TDN] = -0.036\left[\ln\left(\frac{G}{S}\right)\right]^2 - 0.157ln\left(\frac{G}{S}\right) + 1.534 \quad (7)$$

$$[TDN] = -0.0134\left[\ln\left(\frac{P}{S}\right)\right]^2 + 0.203ln\left(\frac{P}{S}\right) + 0.797 \quad (8)$$

$$[TN] = -0.071\left[\ln\left(\frac{G}{S}\right)\right]^2 - 0.374ln\left(\frac{G}{S}\right) + 2.630 \quad (9)$$

$$[TN] = -0.036\left[\ln\left(\frac{P}{S}\right)\right]^2 + 0.380ln\left(\frac{P}{S}\right) + 1.737 \quad (10)$$

It is closely related to the source of C in TSP that stable C isotope composition of total carbon ($\delta^{13}C$) has a significant declining trend before rising with the increment of human activities intensity (Fig. 4a and d). $\delta^{13}C$ is much lower in emissions from human activities than in nature (Peng et al., 1983), especially in the form of inorganic carbonates. Therefore, in contrast to the inverted U curve of TC content, $\delta^{13}C$ presents a U-shaped trend. The $\delta^{15}N$ in TSP showed a rapid increase before stabilizing following increasing human activities intensity (Fig. 4b and e, Eqs. 11–12). The increment indicates that human activities emit nitrogenous substances high in $\delta^{15}N$ into the atmosphere (Ren et al., 2017). At the same time, the stabilizing trend infers that, in addition to local sources, N can also be transported from surrounding regions (as discussed below).

$$\delta^{15}N = 0.810ln\left(\frac{G}{S}\right) + 8.959 \quad (11)$$

$$\delta^{15}N = 0.764ln\left(\frac{P}{S}\right) + 3.484 \quad (12)$$

In contrast with the clear inverted-U pattern for TC, WSOC, TN, and TDN, the concentrations of NH_4^+, NO_3^- and SO_4^{2-} in TSP keep increasing with GDP and population density (Fig. 4c and f, Eqs. 13–18). Only after reaching a certain level will they be stabilized. This is because these ions in TSP mainly originate from the chemical conversion of ammonia (NH_3), nitrogen oxides (NO_x), and sulfur dioxide (SO_2) (An et al., 2019). Although the C and N content of the TSP in the developed areas that we have previously studied has a downward trend, the NH_3, NO_x, and SO_2 from nearby regions can be easily transported to these developed areas, thereby maintaining the concentrations of NH_4^+, NO_3^- and SO_4^{2-} at a high level. This phenomenon enlightens us that reducing air pollutants should focus not only locally but also jointly reduce emissions in a large area to achieve coordinated control.

$$\left[NH_4^+\right] = 0.147ln\left(\frac{G}{S}\right) + 1.773 \quad (13)$$

$$\left[NH_4^+\right] = 0.168ln\left(\frac{P}{S}\right) + 0.649 \quad (14)$$

$$\left[SO_4^{2-}\right] = 0.608ln\left(\frac{G}{S}\right) + 6.068 \quad (15)$$

$$\left[SO_4^{2-}\right] = 0.609ln\left(\frac{P}{S}\right) + 1.800 \quad (16)$$

$$\left[NO_3^-\right] = 0.200ln\left(\frac{G}{S}\right) + 2.447 \quad (17)$$

$$\left[NO_3^-\right] = 0.215ln\left(\frac{P}{S}\right) + 0.976 \quad (18)$$

3.2 Water

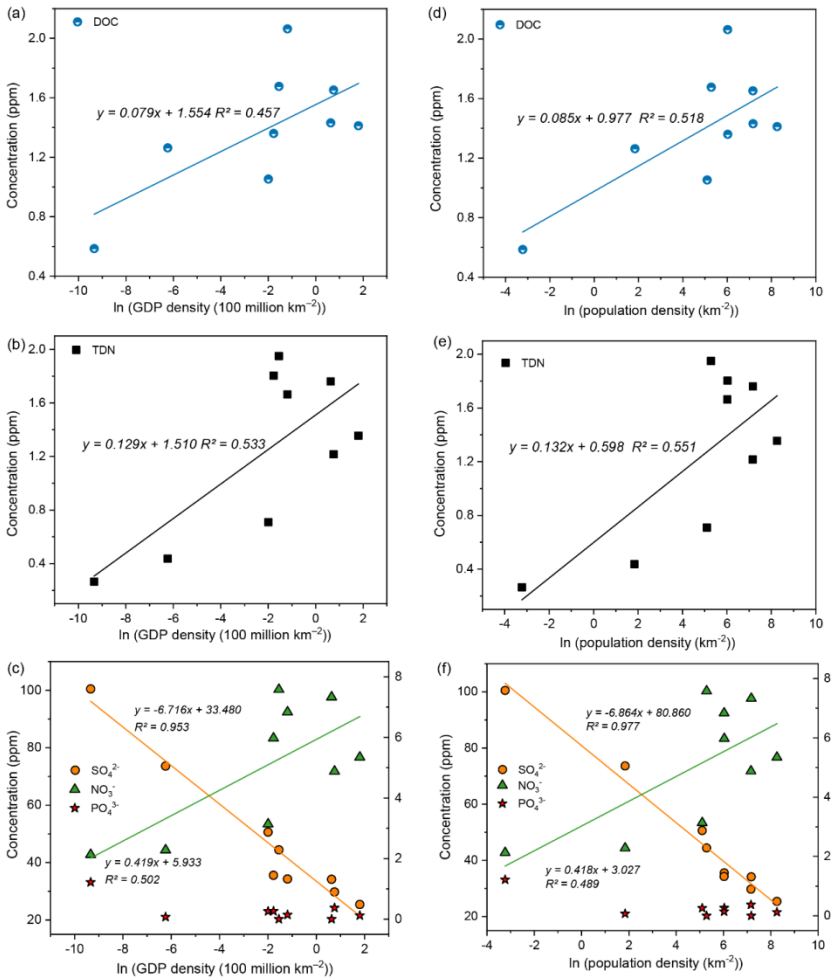

Figure 5 Relationships between (a) DOC, (b) TDN, (c) SO42–, NO3– and PO43– in water samples and ln (GDP density); (d) DOC, (e) TDN, (f) SO42–, NO3– and PO43– in water samples and ln (population density).

For DOC, TDN, and NO_3^- in water, their contents have a clear upward trend with increasing GDP density and population density (Fig. 5, Eqs. 19–24). This may be attributed to two reasons. On the one hand, the developed areas of the YRB are mainly located in the middle and lower reaches and the estuary, while the underdeveloped areas are mainly located in the source and upper reaches of the Yangtze River. The concentrations of DOC, TDN, and NO_3^- in the water increase from upper to lower reaches with the accumulation of these components. On the other, human activities are more intense in the lower reaches, discharging more substances containing biogenic elements into the Yangtze River, thus significantly increasing the concentration of C and N. However, the trends of SO_4^{2-} changes exclude the first cause from being the main reason. There is a good negative correlation between SO_4^{2-} concentration in water and human activities intensity (Eqs. 25 and 26). This is due to the severe soil salinization in the source area of the Yangtze River with few human activities (Zhang et al., 2013), where a large amount of SO_4^{2-} is lost from the soil and discharged into the water, leading to its high concentration. As the river flows to the estuary, precipitation and surface runoff in the YRB increase, diluting the SO_4^{2-} concentration, resulting in low SO_4^{2-} content in water in developed areas downstream. Therefore, dilution makes it impossible for C and N concentrations to increase only through accumulation from upstream.

$$[DOC] = 0.079 ln\left(\frac{G}{S}\right) + 1.554 \quad (19)$$

$$[DOC] = 0.085 ln\left(\frac{P}{S}\right) + 0.977 \quad (20)$$

$$[TDN] = 0.129 ln\left(\frac{G}{S}\right) + 1.510 \quad (21)$$

$$[TDN] = 0.132ln\left(\frac{P}{S}\right) + 0.598 \quad (22)$$

$$\left[NO_3^-\right] = 0.419ln\left(\frac{G}{S}\right) + 5.933 \quad (23)$$

$$\left[NO_3^-\right] = 0.418ln\left(\frac{P}{S}\right) + 3.027 \quad (24)$$

$$\left[SO_4^{2-}\right] = -6.716ln\left(\frac{G}{S}\right) + 33.480 \quad (25)$$

$$\left[SO_4^{2-}\right] = -6.864ln\left(\frac{P}{S}\right) + 80.860 \quad (26)$$

The primary reason for the increase in DOC, TDN, and NO_3^- content in water is the increasing population and the discharge of more anthropogenic C- and N-containing substances into the water. Although the concentrations of these components present a linear relationship with the logarithm of GDP density or population density, it is evident that they have stabilized or even declined in some areas with high population density and GDP density. Therefore, although the content of these components in the water does not show a prominent inverted U curve like the TC, WSOC, TN, and TDN in atmospheric TSP, it already has the embryonic form of such patterns. The EEM spectra (Fig. 6) also indicate that organic matter contents in water from Tanggula and Batang are considerably low. The increase of fluorescence intensity results from the increasing population size, especially in those industrial cities such as Luzhou and Chongqing. With further development of the economy, the fluorescence intensity of water tends to stabilize. In other words, with the economic and social developments, the water quality in the entire YRB is further improved, and the upstream area's discharge on the downstream area's water quality is reduced, possibly making the appearance of the inverted U curve more apparent. However, PO_4^{3-} concentration in water is affected by various factors, such as dilution, anthropogenic discharge, and precipitation removal, resulting in a low content with no significant correlation with either GDP density or population density (Fig. 5c and f).

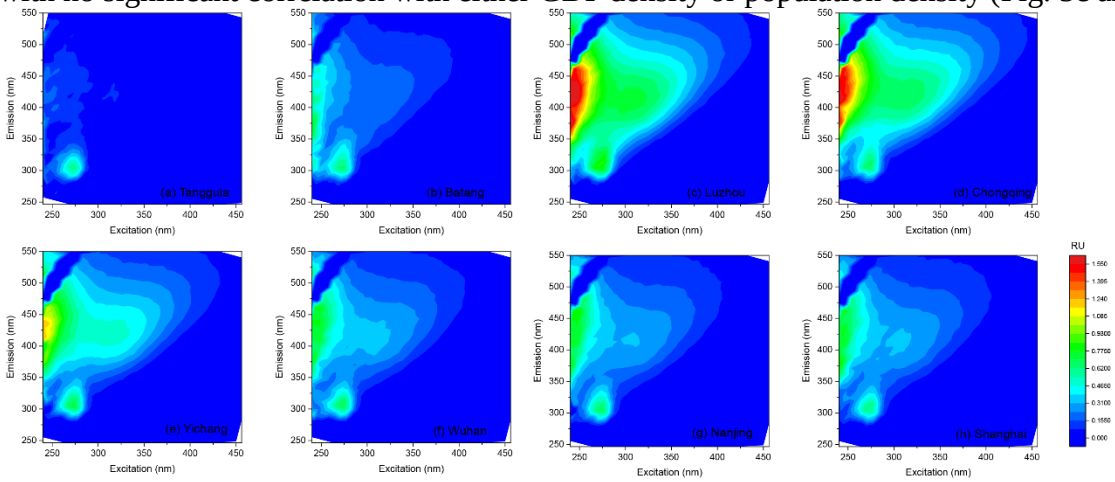

Fig.6 The Excitation-Emission-Matrix (Eem) Spectra of the Water Samples.

3.3 Soil

Since the substances in the soil are unlikely to be transported from other regions like those in the atmosphere and water, the physical and chemical properties of the soil reflect more on the local characteristics, including natural characteristics and the degree of human influence. For soil samples, the contents of DOC, SO_4^{2-} and NO_3^- show good positive correlations with GDP density and population density (Fig. 7, Eqs. 27–32). Although natural conditions, including parent material, topography, climate, vegetation, and pedogenesis time, can affect soil's physical and chemical properties, these positive correlations still prove the critical role of human activities. Biogenic elements such as C, N, and S are necessary for the maintenance of human livelihoods. In return, the

increase in the intensity of human activities will inevitably release the substances containing these biogenic elements into the natural environment. Whether discharged into the atmosphere, water, or soil, these substances will eventually enter the soil and be preserved, resulting in positive correlations between the contents of these substances and the intensity of human activities. Unlike DOC, SO_4^{2-} and NO_3^-, the content of PO_4^{3-} remains at a stable low level. This may be due to the lower mobility of PO_4^{3-}, PO_4^{3-} emitted by human activities is mainly in agricultural production areas instead of the riparian area where soil samples were collected. Besides, the EEM spectra of soil extraction (Fig. 8) suggest that the soil organic matter contents in Tanggula and Batang are very low. However, in other regions, there is no significant trend of changes with population growth, showing that soil organic matter is largely affected by soil parent material and other natural factors.

$$[DOC] = 0.242ln\left(\frac{G}{S}\right) + 4.260 \quad (27)$$

$$[DOC] = 0.240ln\left(\frac{P}{S}\right) + 2.588 \quad (28)$$

$$\left[SO_4^{2-}\right] = 0.046ln\left(\frac{G}{S}\right) + 0.714 \quad (29)$$

$$\left[SO_4^{2-}\right] = 0.039ln\left(\frac{P}{S}\right) + 0.429 \quad (30)$$

$$\left[NO_3^-\right] = 0.038ln\left(\frac{G}{S}\right) + 0.620 \quad (31)$$

$$\left[NO_3^-\right] = 0.039ln\left(\frac{P}{S}\right) + 0.351 \quad (32)$$

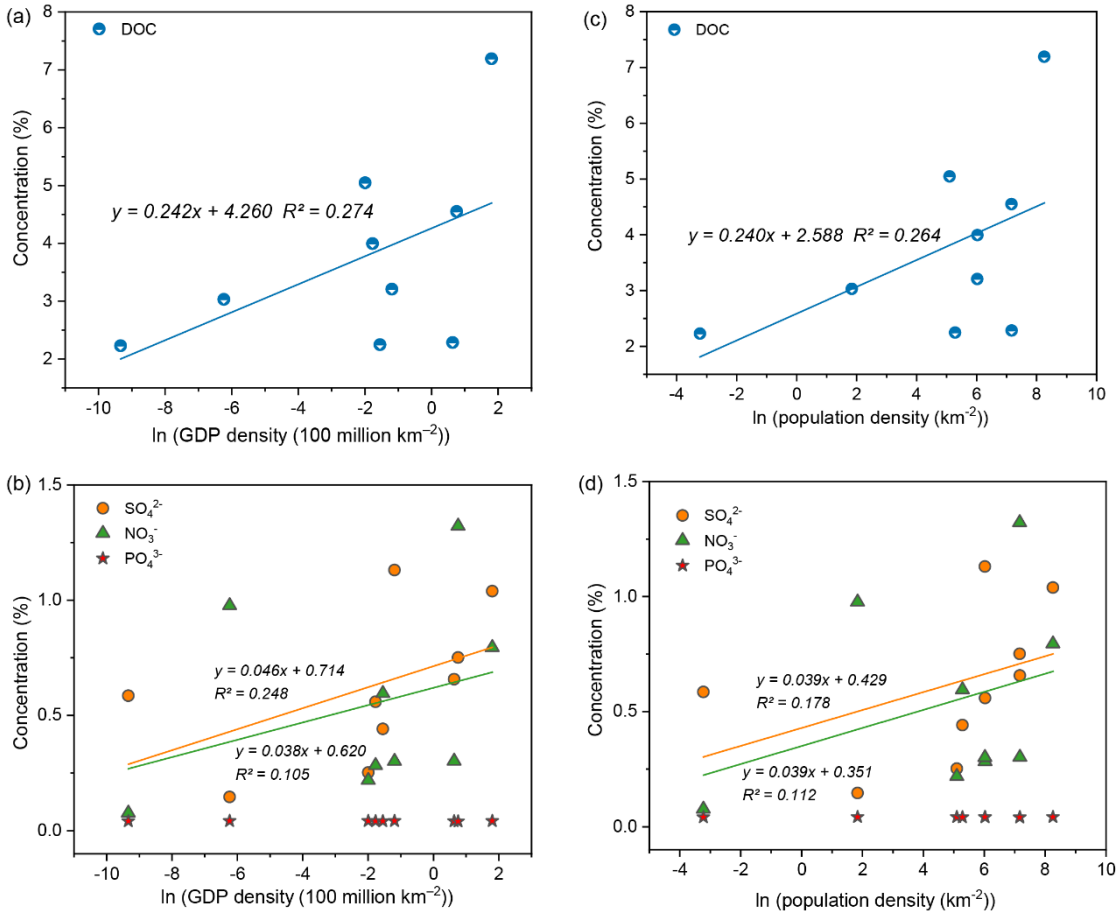

Fig.7 Relationships between (a) Doc, (B) So42–, No3– and Po43– in Soil Samples and Ln (Gdp Density); (C) Doc, (d) So42–, No3– and Po43– in Soil Samples and Ln (Population Density).

Unlike air and water pollution control that have immediate effects, soil control is more complicated. First, the source of materials in the soil is complex, including direct emissions, atmospheric deposition, and surface runoff. Second, the soil has a wide distribution range and lacks fluidity. Third, removing materials in the soil requires better technology, higher costs, and longer time. As can be seen from Fig. 7, the contents of the studied substances have been increasing with GDP density and population density, without any decreasing or stable trend, which is different from the results of TSP or water. Therefore, it can be speculated that with the increase in human activities intensity and economic development, the concentrations of biogenic elements in the soil of the YRB will further increase. Fortunately, the environmental hazards caused by the biogenic elements in the soil are not as high as the biogenic elements in the atmosphere and water. Under such circumstances, the current concern about soil quality should be more concerned with the content of heavy metals and persistent organic pollutants (POPs) rather than biogenic elements.

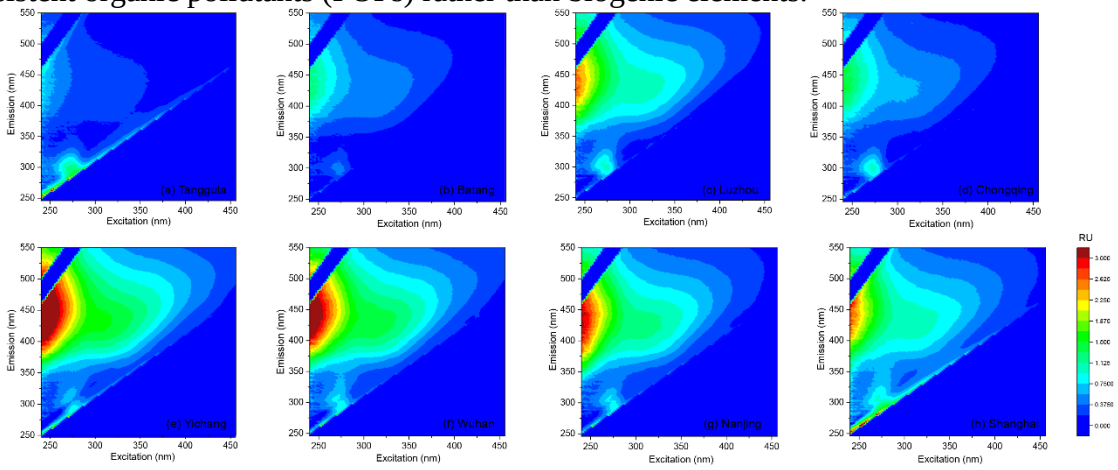

Fig.8 The Excitation-Emission-Matrix (Eem) Spectra of the Soil Samples.

3.4 Implications

The leading indicators in atmospheric TSP, water, and soil show different functional relationships with GDP density or population density. For TSP, there is an inverted U-curve relationship between the leading test indicators and the intensity of human activities, telling us that the degree of air pollution in most areas of the YRB has crossed the peak, showing a trend of air quality improvement. To determine the degree of economic development when the air pollution is the most serious, the abscissa corresponding to the peak of the fitted quadratic function is calculated to obtain the average and standard deviation (Eqs. 33 and 34, μ and σ mean the average and standard deviation (SD) of x_1, x_2, ... and x_n, respectively).

$$\mu = \frac{x_1 + x_2 + \ldots + x_n}{n} = \frac{\sum_{i=1}^{n} x_i}{n} \quad (33)$$

$$\sigma = \sqrt{\frac{1}{n}\sum_{i=1}^{n}\left(x_i - \mu\right)^2} \quad (34)$$

According to Eqs 3, 5, 7, 9, 33, and 34, the natural logarithm of GDP density at the peak of air pollution is –0.256 ± 0.322 (average ± SD), so the average GDP density is 0.0769 (0.0568 ~ 0.1040, 1 SD) *100 million m^{-2}. Similarly, from Eqs 4, 6, 8, 10, 33, and 34, the natural logarithm of the population density at the peak of air pollution is 5.334 ± 1.595 (average ± SD), so the average GDP density is 207.32 (42.05 ~ 1022.14, 1 SD) m^{-2}. In other words, the per capita GDP when the air pollution is the most serious is G/P = 10^8*0.0769/ 207.32 = 37, 092 Yuan. According to China's per capita GDP data and the national average $PM_{2.5}$ concentration data in recent years (Fig. 9, Shi et al., 2020), per capita GDP exceeded 37, 092 Yuan and reached 39, 874 Yuan for the first time in 2012 (National Bureau of Statistics of China, 2020), while the $PM_{2.5}$ concentration reached its peak in 2013 and began to decline thereafter. Therefore, this study has a good simulation of the relationship between air quality concentration and the level of economic development.

The changes in water and soil quality data are different from those of the atmosphere. The water quality of the Yangtze River has been relatively stable in the developed middle and lower reaches, indicating that the current pollution level of the river has reached its peak. It is predicted that the water quality will gradually improve with further development of the economy in the future. The soil's content of biogenic elements such as C, N, S, and P is still rising. It is speculated that it has not reached the environmental capacity and therefore cannot be counted as a pollutant. The current soil pollutants may still be heavy metals and POPs. However, with the further increase in human activities intensity, it will cause harm to the ecological environment and become a pollutant. By then, soil pollution prevention and control need to consider the content of biogenic elements.

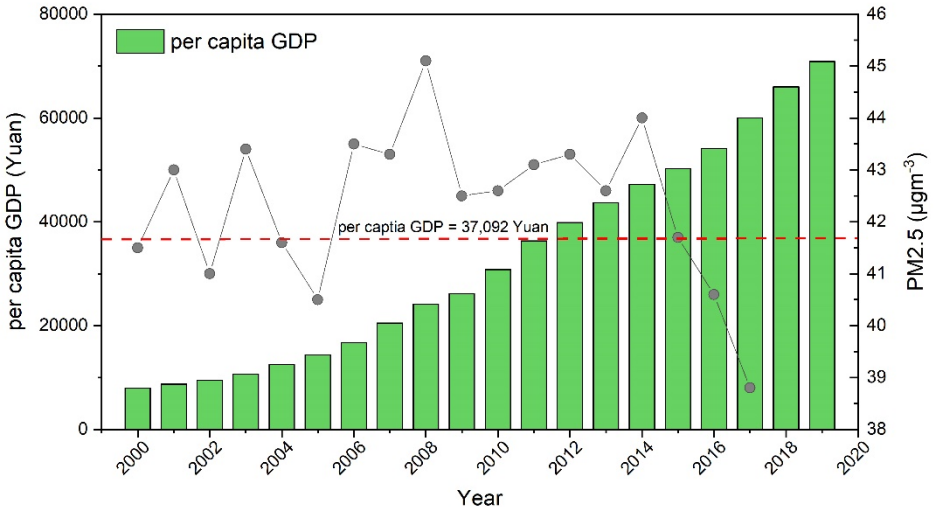

Fig.9 The Average Per Capita Gdp and Pm2.5 Concentrations in China in Recent Years (National Bureau of Statistics of China, 2020; Shi et al., 2020).

4. Conclusion

The intensity of human activities has a significant impact on the content of biogenic elements in the natural environment. For the YRB, with the increase of local population and GDP, the concentration of biogenic elements in the atmosphere shows a trend of first rising and then falling, which is in line with the Kuznets inverted U-shaped curve hypothesis and the inverted U curve of environmental pollution. The per capita GDP corresponding to the peak value of the inverted U curve obtained in this study is 37,092 Yuan. Based on this, it is speculated that the air quality in the YRB and the whole country has already passed this peak value and is on the right side of the inverted U curve. The changes in the content of biogenic elements in water indicate that the level of water pollution in the Yangtze River stays at its peak. The changes in the content of soil biogenic elements indicate that the concentration of biogenic elements in the soil of the YRB is low and has not caused significant environmental pollution. From the perspective of biogenic elements, the soil quality is on the left side of the inverted U curve and is far from the peak. Overall, with the development of the economy, the sequence of environment treatment is: air first, water second, and soil last.

Acknowledgment

The author sincerely acknowledges Tianjin University and the Institute of Atmospheric Physics, Chinese Academy of Sciences for their assistance in field sampling and experimental analyses. The author also thanks Prof. Pingqing Fu, Dr. Libin Wu, and Dr. Shuang Chen from Tianjin University for their guidance and help.

References

[1] An Z., Huang R.-J., Zhang R., Tie X., Li G., Cao J., Zhou W., Shi Z., Han Y., Gu Z., Ji Y. 2019. Severe haze in northern China: A synergy of anthropogenic emissions and atmospheric processes. Proceedings of the National Academy of Sciences of the United States of America 116 (18): 8657–8666.

[2] Chai Liwei, Huang Muke, Fan Hao, Wang Jie, Jiang Dalin, Zhang Mengjun, Huang Yi. 2018. Urbanization altered regional soil organic matter quantity and quality: insight from excitation emission matrix (EEM) and parallel factor analysis (PARAFAC). Chemosphere 220: 249–258.

[3] Cheng Borong, Yue Siyao, Hu Wei, Ren Lujie, Deng Junjun, Wu Libin, Fu Pingqing. 2020. Summertime fluorescent bioaerosol particles in the coastal megacity Tianjin, North China. Science of the Total Environment 723: 137966.

[4] Chongqing Municipal Bureau of Statistics & Survey Office of the National Bureau of Statistics in Chongqing. 2020. Chongqing Statistical Yearbook 2020 (in Chinese). China Statistics Press, Beijing.

[5] Cole M. A., Rayner A. J., Bates J. M. 1997. The environmental Kuznets curve: An empirical analysis. Environment and Development Economics 2 (4): 401–416.

[6] Daniel A. Lashof, Dilip R. Ahuja. 1990. Relative contributions of greenhouse gas emissions to global warming. Nature 344: 529–531.

[7] Dasgupta Susmita, Laplante Benoit, Wang Hua, Wheeler David. 2002. Confronting the environmental kuznets curve. Journal of Economic Perspectives 16 (1): 147–168.

[8] Dawood D. H., Sanad M. I. 2014. Determination of ions (anion and cation) by ion chromatography in drinking water from Talkha territory and some its villages, Dakahlia, Egypt. Journal of Agricultural Chemistry and Biotechnology 5 (9): 215–226.

[9] Galitskova Y. M., Murzayeva A. I. 2016. Urban soil contamination. Procedia Engineering 153: 162–166.

[10] Gorham E., Vitousek P. M., Reiners W. A. 1979. The regulation of chemical budgets over the course of terrestrial ecosystem succession. Annual Review of Ecology and Systematics 10: 53–84.

[11] Haygarth P. M., Warwick M. S., House W. A. 1997. Size distribution of colloidal molybdate reactive phosphorus in river waters and soil solution. Water Research 31 (3): 439–448.

[12] Holme A. 2010. The Great River Civilizations. Springer Berlin Heidelberg.

[13] Huang Ru-Jin, Yanlin Zhang, Carlo Bozzetti, Kin-Fai Ho, Jun-Ji Cao, Yongming Han, Kaspar R. Daellenbach, Jay G. Slowik, Stephen M. Platt, Francesco Canonaco, Peter Zotter, Robert Wolf, Simone M. Pieber, Emily A. Bruns, Monica Crippa, Giancarlo Ciarelli, Andrea Piazzalunga, Margit Schwikowski, Gülcin Abbaszade, Jürgen Schnelle-Kreis, Ralf Zimmermann, Zhisheng An, Sönke Szidat, Urs Baltensperger, Imad El Haddad, André S. H. Prévôt. 2014. High secondary aerosol contribution to particulate pollution during haze events in China. Nature 514 (7521): 218–222.

[14] Hubei Provincial Bureau of Statistics & Survey Office of the National Bureau of Statistics in Hubei. 2020. Hubei Statistical Yearbook 2020 (in Chinese). China Statistics Press, Beijing.

[15] Humborg C., Mörth C.-M., Sundbom M., Wulff F. 2007. Riverine transport of biogenic elements to the Baltic Sea: Past and possible future perspectives, Hydrology and Earth System Sciences 11: 1593–1607.

[16] Jiangsu Provincial Bureau of Statistics & Survey Office of the National Bureau of Statistics in Jiangsu. 2020. Jiangsu Statistical Yearbook 2020 (in Chinese). China Statistics Press, Beijing.

[17] Karanfil T., Erdogan I., Schlautman M. A. 2003. Selecting filter membranes for measuring DOC and UV_{254}. American Water Works Association 95 (3): 86–100.

[18] Karr J. R., Chu E. W. 2000. Introduction: Sustaining living rivers. Hydrobiologia 422: 1–14.

[19] Lu C., Tian H. 2017. Global nitrogen and phosphorus fertilizer use for agriculture production in the past half century: Shifted hot spots and nutrient imbalance. Earth System Science Data 9: 181–192.

[20] National Bureau of Statistics of China. 2020. China Statistical Yearbook 2020 (in Chinese). China Statistics Press, Beijing.

[21] Peng T. H., Broecker W. S., Freyer H. D., Trumbore, S. 1983. A deconvolution of the tree ring based $\delta^{13}C$ record. Journal of Geophysical Research - Oceans 88: 3609–3620.

[22] Pinto U., Maheshwari B., Shrestha S., Morris C. 2012. Modelling eutrophication and microbial risks in peri-urban river systems using discriminant function analysis. Water Research 46 (19): 6476–6488.

[23] Qinghai Provincial Bureau of Statistics & Survey Office of the National Bureau of Statistics in Qinghai. 2020. Qinghai Statistical Yearbook 2020 (in Chinese). China Statistics Press, Beijing.

[24] Ren H. J., Chen Y. C., Wang X. T., Wong G., Cohen A. L., Decarlo T. M., Weigand M. A., Mii H. S., Sigman D. M. 2017. 21st-century rise in anthropogenic nitrogen deposition on a remote coral reef. Science 356 (6339): 749–752.

[25] Shi Yan, Liu Ruimei, Luo Yi, Yangkun. 2020. Spatiotemporal variations of $PM_{2.5}$ pollution evolution in China in recent 20 years. Environmental Science 41 (1): 1–13 (in Chinese with English abstract).

[26] Sichuan Provincial Bureau of Statistics & Survey Office of the National Bureau of Statistics in Sichuan. 2020. Sichuan Statistical Yearbook 2020 (in Chinese). China Statistics Press, Beijing.

[27] Shanghai Municipal Bureau of Statistics & Survey Office of the National Bureau of Statistics in Shanghai. 2020. Shanghai Statistical Yearbook 2020 (in Chinese). China Statistics Press, Beijing.

[28] Smith V. H., Schindler D. W. 2009. Eutrophication science: Where do we go from here? Trends in Ecology & Evolution 24 (4): 201–207.

[29] Song J. M. 2010. Biogeochemical Processes of Biogenic Elements in China Marginal Seas. Springer-Verlag, GmbH & Zhejiang University Press, Dordrecht, London New York & Hangzhou.

[30] Streets D. G., Waldhoff S. T. 2000. Present and future emissions of air pollutants in China: SO_2, NO_x, and CO. Atmospheric Environment 34 (3): 363–374.

[31] Violante F. S., Barbieri A., Curti S., Sanguinetti G., Graziosi F., Mattioli S. 2006. Urban atmospheric pollution: Personal exposure versus fixed monitoring station measurements. Chemosphere 64 (10): 1722–1729.

[32] Volk C., Wood L., Johnson B., Robinson J., Zhu H. W., Kaplan L. 2002. Monitoring dissolved organic carbon in surface and drinking waters. Journal of Environmental Monitoring 4 (1), 43–47.

[33] Wu Libin, Yue Siyao, Shi Zongbo, Hu Wei, Chen Jing, Ren Hong, Deng Junjun, Ren Lujie, Fang Yunting, Yan Hong, Li Weijun, Roy Harrison, Fu Pingqing. 2021. Source forensics of inorganic and organic nitrogen using $\delta^{15}N$ for tropospheric aerosols over Mt. Tai. npj Climate and Atmospheric Science 4: 8.

[34] Zhang Dingfan, Shi Xiaogang, Xu He, Jing Qiaonan, Pan Xicai, Liu Ting, Wang Huanzhi, Hou Huimin. 2020. A GIS-based spatial multi-index model for flood risk assessment in the Yangtze River Basin, China. Environmental Impact Assessment Review 83: 106397.

[35] Zhang Y., Zhang S., Xia J., Dong H. 2013. Temporal and spatial variation of the main water balance components in the three rivers source region, China from 1960 to 2000. Environmental Earth Sciences 68 (4): 973–983.

[36] Zhuo L., Guan X., Ye S. 2020. Prediction analysis of the coordinated development of the sports and pension industries: Taking 11 provinces and cities in the Yangtze River Economic Belt of China as an example. Sustainability 12 (2493): 1–18.